The Effects of STRA6 Regulation of the Circadian Rhythm on Choroidal Neovascularization

Ying Yang,[1,2] Shenglai Zhang,[1,2] Shu Su,[1] Xiaowei Yang,[1] Jia Chen,[1] and Aimin Sang[1]

[1]Eye Institute, Affiliated Hospital of Nantong University, Nantong, Jiangsu, China
[2]Medical School of Nantong University, Nantong, Jiangsu, China

Correspondence: Aimin Sang, Department of Ophthalmology, Affiliated Hospital of Nantong University, Nantong, Jiangsu 226001, China;
sangam@ntu.edu.cn.
Jia Chen, Department of Ophthalmology, Affiliated Hospital of Nantong University, Nantong, Jiangsu 226001, China;
carolcheneye@126.com.

YY and SZ contributed equally to this work.

Received: April 16, 2024
Accepted: August 26, 2024
Published: September 13, 2024

Citation: Yang Y, Zhang S, Su S, Yang X, Chen J, Sang A. The effects of STRA6 regulation of the circadian rhythm on choroidal neovascularization. *Invest Ophthalmol Vis Sci.* 2024;65(11):21. https://doi.org/10.1167/iovs.65.11.21

Purpose. This study aims to investigate the relationship among STRA6, circadian rhythm, and choroidal neovascularization (CNV) formation, as well as the regulatory mechanism of STRA6 in CNV under circadian rhythm disturbances.

Methods. C57BL/6J male mice (aged 6 weeks) were randomly divided into control and jet lag groups (using a time shift method every 4 days to disrupt the molecular clock's capacity to synchronize with a stable rhythm). A laser-induced CNV model was established in both the control and the jet lag group after 2 weeks of jet lag. The size of CNV lesions and vascular leakage were detected by morphological and imaging examination on the seventh day post laser. STRA6 was screened by full transcriptome sequencing. Bioinformatics analysis was conducted to assess the variation and association of STRA6 in the GSE29801 dataset. The effects of STRA6 were evaluated both in vivo and in vitro. The pathway mechanism was further elucidated and confirmed through immunofluorescence of paraffin sections and Western blotting.

Results. The disturbance of circadian rhythm promotes the formation of CNV. Patients with age-related macular degeneration (AMD) exhibited higher levels of STRA6 expression compared to the control group, and STRA6 was enriched in pathways related to angiogenesis. In addition, CLOCK and BMAL1, which are initiators that drive the circadian cycle, had regulatory effects on STRA6. Knocking down STRA6 reversed the promotion of CNV formation caused by circadian rhythm disturbance in vivo, and it also affected the proliferation, migration, and VEGF secretion of RPE cells without circadian rhythm in vitro, as well as impacting endothelial cells. Through activation of the JAK2/STAT3/VEGFA signaling pathway in unsynchronized RPE cells, STRA6 promotes CNV formation.

Conclusions. This study suggests that STRA6 reduces CNV production by inhibiting JAK2/STAT3 phosphorylation after circadian rhythm disturbance. The results suggest that STRA6 may be a new direction for the treatment of AMD.

Keywords: wet age-related macular degeneration (wAMD), choroidal neovascularization (CNV), circadian rhythm, full transcriptome sequencing, STRA6

Age-related macular degeneration (AMD) is the leading cause of irreversible blindness in individuals over 60 years old in developed countries.[1] It significantly impacts quality of life, leading to reduced activity levels and an increased risk of depression or anxiety.[2] Choroidal neovascularization (CNV) is a key feature of advanced wet age-related macular degeneration (wAMD) and a primary contributor to vision loss.[3] Vascular endothelial growth factor (VEGF) plays a pivotal role in its development.[4] Currently, anti-VEGF drugs are commonly used in CNV treatment. Despite their efficacy in reducing abnormal blood vessel formation, only 30% to 40% of patients experience improved vision following intravitreal anti-VEGF therapy, with drug resistance posing a significant obstacle.[5] Consequently, further research into synergistic anti-VEGF therapy is imperative.

The daily rhythm of light/dark cycle is a key zeitgeber (time cue), which plays a critical role in human physiology.[6] Suprachiasmatic nucleus (SCN), as the main biological clock of mammalian circadian rhythm system, transmits signals to tissues and organs by regulating related downstream factors and interacting with endogenous clocks, causing cyclic changes in various indicators of the body.[7–9] The highest and lowest values of expression are separated by about 12 hours and undergo a full cycle within 24 hours.[10] Disruptions to these rhythms, such as frequent shifts between day and night schedules, can heighten the risk of disease. Many diseases caused by pathologic angiogenesis are linked to disturbances in circadian rhythms, underscoring the importance of understanding their impact on disease development. Previous studies have found that core clock proteins are expressed in the outer and inner layers of the retina, but only in the cones' photoreceptors do these proteins show circadian changes.[11,12] Photoreceptors rely on close interaction with the retinal pigment epithelium (RPE) to renew their photosensitive outer segments by shedding continuous

discs,[13,14] a process that represents circadian rhythms.[15] Studies have demonstrated that the RPE exhibits circadian rhythm and is implicated in the pathogenesis of AMD as a major source of VEGF.[16] These findings suggest a significant relationship between circadian rhythm and the development of AMD.

The visual perception of photoreceptors depends on the interaction of light incident photons with retinol (ROL). It is transported in a complex with retinol binding protein (RBP) and delivered to photoreceptors through choroidal blood flow behind the RPE.[17,18] Stimulated by retinoic acid 6 (STRA6) is a multiplex transmembrane region protein that functions as a specific membrane receptor for RBP, exhibiting high affinity in binding RBP and efficient uptake of vitamin A from the ROL-RBP complex.[17] STRA6 is essential for visual response. In the absence of STRA6, the length of the inner and outer segments of rods decreased, and the number of cones decreased, as were scotopic and photopic responses.[19] Studies have indicated a high expression of STRA6 in RPE cells, attributed to the conducive physiological environment for its signal transduction.[20] RPE needs to absorb large amounts of vitamin A for proper visual functions. The point mutations in human STRA6 associated with birth defects cause severe or complete loss of vitamin A uptake activity from holo-RBP.[21] Vitamin A affects the body's subjective response to day and night, which in turn affects the biological clock.[22] In addition, STRA6 expresses the circadian rhythm and regulates diurnal insulin responses.[23] However, excessive intake of ROL can lead to an increase in all-trans ROL, a pro-angiogenic factor that interacts with RPE cell base side via the STRA6 protein and is a potential risk factor for wet AMD.[24] The relationship among STRA6, circadian rhythm, and CNV formation requires further investigation.

Numerous studies have demonstrated the significant involvement of the Janus kinase 2 (JAK2)/signal transduction and activator of transcription 3 (STAT3) signaling pathway in angiogenesis.[25] Furthermore, VEGFA, a crucial factor in the regulation of angiogenesis, has been identified as a downstream target gene of this pathway.[25–27] The binding of STRA6 to RBP can lead to the recruitment and activation of JAK2, facilitating the nuclear translocation of STAT3.[20] Moreover, the overexpression of JAK2 was observed to enhance retinol uptake only in the presence of STRA6.[28] Our GSVA pathway enrichment analysis indicates that STRA6 is linked to lipid metabolism, and this change in function is associated with increased JAK2/STAT3 signal transduction.[29] Based on these findings, it is hypothesized that STRA6 may promote angiogenesis by upregulating VEGFA through the JAK2/STAT3 pathway.

Our study revealed a significant increase in CNV following circadian rhythm disturbance. At the same time, the expression of STRA6 and VEGFA was significantly upregulated, and they had similar expression conditions. Knocking down STRA6, both in vivo and in vitro, resulted in a reduction in the range of ocular lesions, as well as in the migration and proliferation of RPE cells and endothelial cells. These findings provide compelling evidence for the involvement of STRA6 in regulating angiogenesis in the context of circadian dysregulation and suggest that mitigating the effects of circadian rhythms via the STRA6/JAK2/STAT3/VEGFA signaling pathway may be a therapeutic strategy to prevent the development of CNV.

Materials and Methods

Ethics Statement

The animal studies were approved by the Ethics Committee of Animal Experiments at Nantong University (Nantong, China; approval ID: S20220822-902), and all the processes were in strict accordance with the Standard Operating Procedures for Laboratory Animal Center of NTU. All methods were reported in accordance with the ARVO Animal Statement.

Mouse Model of Circadian Rhythm and Jet Lag

Six-week-old male C57BL/6J mice were provided by Shanghai SLAC Laboratory Animal Co., Ltd. (Shanghai, China). All the mice were randomly divided into two groups: the circadian rhythm group and the jet lag group, after being acclimated to natural diurnal cycle conditions for 1 week. The circadian rhythm group was exposed to 300 Lux of light from 8:00 (zeitgeber time 0 [ZT0]) to 20:00 (zeitgeber time 12 [ZT12]) and kept in darkness from 20:00 to 8:00 to mimic a consistent day-night cycle.[30,31] The jet lag group experienced an 8-hour forward shift every 4 days, relative to the normal 12/12-hour cycle.[32] This protocol was followed for an additional 3 weeks.

Mouse CNV Model

Each mouse was anesthetized with a 0.15 mL intraperitoneal injection of a 1% pentobarbital sodium (50 mg/kg). Following complete anesthesia, the eyes were dilated using compounded tropicamide eye drops. Topical anesthesia with proparacaine hydrochloride eye drops was applied to keep the cornea moist with sodium hyaluronate. The 532 nm frequency-doubling laser, with a spot size of 100 µm, power of 100 mW, and duration of 150 ms, from the multi-wavelength Kryptonion fundus treatment laser (Coherent, USA) was utilized for laser photocoagulation. This was carried out at the 3, 6, 9, and 12 o'clock positions around the mouse optic disc, approximately one optic disc diameter apart.

Fundus Fluorescein Angiography

Mice were anaesthetized by intraperitoneal injection on days 3, 7, 14, and 21 following laser photocoagulations. Two percent concentration of 10% sodium fluorescein diluted with PBS was administered at a volume of 0.1 mL per injection. Fundus angiographic leakage was observed and sequential real-time fundus fluorescein angiography (FFA) images were captured with Saris Multi-Modal Ophthalmic Imaging System for Animal (Robotrak, China) 1 to 2 minutes after fluorescein injection post-injection.

Optical Coherence Tomography Angiography

The mice were anesthetized with 0.5% sodium pentobarbital by intraperitoneal injection and the eyes were dilated using compound tropicamide eye drops. After 10 minutes, the thickness, area, and central abnormal blood flow of the lesion were photographed via 400 kHz SS-OCTA instrument (BM400K; TowardPi Medical Technology Co., Ltd., Beijing, China). Optical coherence tomography angiography (OCTA) data were obtained with a raster scan protocol of 1536 (hori-

Investigative Ophthalmology & Visual Science

zontal) × 1280 (vertical) B-scans. We scanned the BOTTOM-RPE layer and observed blood flow imaging in the capillary-free layer of the choroid. The thickness and area were quantified in the OCTA machine. The measurement position was always centered at the fovea without any rotation and the data from the left eyes were horizontally flipped for statistical analysis. Abnormal blood flow areas were quantified using ImageJ software (National Institutes of Health, USA). All the data were analyzed using GraphPad Prism software (version 9.5.1).

Mouse Intravitreal Injection

Cholesterol modified si-STRA6 and si-NC (Servicebio, China) were injected intravitreal in the eyes of CNV mice with a Hamilton syringe (Sigma-Aldrich, Allentown, PA, USA) at a rate of 0.1 nm per mouse on the first day after laser photocoagulation. After anesthesia and immobilization, the mice were treated with eye disinfection, dilation, and topical anesthetic. The needle was inserted vertically at 1 mm behind the corneal limbus and tilted away from the lens. After completing the injection, and waiting for about 10 seconds, we used aureomycin eye cream to prevent infection. The sequences of the primers used are shown in Supplementary Document S1.

Western Blotting

Following dissection and extraction of the mouse RPE-choroid-sclera complex, protein extract was prepared using RIPA buffer supplemented with a protease inhibitor mixture (Thermo, USA). The protein concentration was quantified utilizing a BCA protein assay (Thermo Fisher Scientific, Waltham, MA, USA). Subsequently, electrophoresis was performed on a 10% SDS-polyacrylamide gel, followed by transfer to a PVDF membrane (Merck, Darmstadt, Germany) and blocking with 5% skim milk for 2 hours. The primary antibody was then incubated overnight at 4°C, followed by incubation with the secondary antibody at room temperature for 2 hours. Detection of immune complexes was achieved using a chemiluminescence kit (SuperSignal ECL Kit; Thermo Fisher, USA). The mean intensity (intensity/area) of bands was determined and normalized against α-Tubulin using ImageJ software (National Institutes of Health, USA), and the experiment was independently repeated three times. STRA6 antibody was purchased from Novus (1:500; USA). BMAL1, JAK2, P-JAK2, STAT3, P-STAT3 antibodies were purchased from Cell Signaling Technology, Inc. (1:1000; USA). The CLOCK antibody was purchased from Abcam (1:2000; USA). VEGFA and α-Tubulin antibodies were purchased from Proteintech (1:1000; China). All the data were analyzed using GraphPad Prism (version 9.5.1) software.

Hematoxylin and Eosin Staining

Following removal of mouse eyeballs, fixation was carried out with 4% paraformaldehyde (PFA) at 4°C overnight (approximately 12 hours). Subsequently, dehydration was performed using a series of sucrose solutions with concentrations of 5%, 10%, 20%, and 30% for 4 hours each at 4°C. Once dehydration was completed, embedding in paraffin wax was conducted with the eye axis positioned horizontally, followed by vertical sectioning using a laser. The sections were then subjected to roasting at 65°C, dewaxing, dehydration, and staining with hematoxylin and eosin (H&E). Finally, the samples were sealed with resin and imaged using a Leica Thunder high-resolution fluorescence microscope.

Fluorescence Staining of Choroidal Slides

After the mouse eyeballs were fixed with 4% paraformaldehyde (Beyotime, China) for 2 hours, the cornea, iris, lens, and vitreous were removed, and the RPE-choroid-sclera complex was preserved. After permeabilization with 2% Triton (Sigma-Aldrich, USA) and 5% BSA (Saiguotech, China) for 30 minutes, the tissues were incubated with primary antibodies overnight at 4°C. The tissues were removed from the refrigerator the next day and washed 3 times with PBS (Servicebio, China) for 10 minutes each time. Next, the tissues were incubated with the fluorescent secondary antibody at room temperature for 2 hours. The RPE-choroid-sclera complexes were removed superfluous liquid, flat-mounted onto glass slides. Avoid light throughout the above process. A DAPI-containing anti-fluorescence-quenched sealing tablet (SouthernBiotech, USA) was dripped on the slide, and images were taken with the Nikon Spatial Array Confocal (NSPARC) detector (Nikon, Japan). Image J software (National Institutes of Health, USA) was used to analyze the fluorescence images. All the data were analyzed using GraphPad Prism software (version 9.5.1). CD31 antibody was purchased from R&D Systems (1:15; USA). IB4 antibody was purchased from Vector (1:200; USA). Fluorescent secondary antibody of donkey anti-goat was purchased from Abcam (1:200; USA).

RNA Extraction and Quantitative PCR

After the mouse RPE-choroid-sclera complex was dissected, total RNA was isolated with Trizol (Invitrogen, USA), chloroform, isopropyl alcohol, and other reagents. First strand cDNA was synthesized by reverse transcription from 1 µg total RNA using PrimeScript RT Master Mix Kit (TaKaRa, Japan). Using Fast SYBR Premix EX Taq II (TaKaRa, Japan) for ABI Prism 7900 RT-qPCR (Applied Biosystems Inc., USA), and the relative expression levels were calculated using the relative quantization $2^{-\Delta\Delta CT}$ method. Primers were purchased from Shanghai Sangong Biotechnology (Shanghai, China), and the primer used was as follows:

STRA6-Forward primer: 5′-AGACAGGCAGGAGGTGGTA GAG-3′;
STRA6-Reverse primer: 5′-CGGATCAGGAGCAGGAAG GTTG-3′.
GAPDH-Forward primer: 5′-GGTTGTCTCCTGCGAC TTCA-3′;
GAPDH-Reverse primer: 5′-TGGTCCAGGGTTTCTTAC TCC-3′.

Immunofluorescence of Paraffin section of Eyeball

The paraffin slices were baked in the oven at 65 degrees for 3 hours. Dewaxing was done with xylene and hydration with 100% to 75% alcohol and distilled water. Antigen repair was performed with sodium citrate antigen repair solution (pH 6.0) at 95 degrees to 100 degrees temperature for 20 minutes. Then, they were soaked in 0.5% Triton X-100 and 3% H2O2 at room temperature. Then, sealed with 5% BSA at room temperature for 1 hour. After incu-

Investigative Ophthalmology & Visual Science

bating the primary antibody at 4 degrees overnight, they were incubated with the corresponding secondary antibody at room temperature and away from light for 2 hours. The tablets were sealed with anti-fluorescence quenching solution SouthernBiotech (USA) containing DAPI. The images were taken with the Leica Thunder high resolution fluorescence microscope. IB4 antibody was purchased from Vector (1:200; USA). STRA6 antibody was purchased from Novus (1:500; USA). F4/80 antibody was purchased from Servicebio (1:500; China). Fluorescent secondary antibody of goat anti-mouse and goat anti-rabbit was purchased from Abcam (1:200; USA).

Cells

The human retinal pigment epithelial cell line ARPE-19 was purchased by the Eye Institute of Affiliated Hospital of Nantong University from Shanghai Enzyme Research Biotechnology Co., LTD. (Shanghai, China). HUVEC and RF/6A cells were obtained from ATCC (Manassas, VA, USA). ARPE-19 and HUVEC were maintained in Dulbecco's modified Eagle's medium (DMEM)/F12 medium nutrient Mixture F-12 (Ham's; 1:1) with L-Glutamine and Sodium Pyruvate, with Hepes 15 mM DMEM: F12 (1:1) supplemented with 10% fetal bovine serum (FBS; Gibco, Rockville, MD, USA) and 100 U/mL penicillin-streptomycin mixture (Gibco, USA) at 37°C in 5% CO2. RF/6A cells were grown in EMEM containing 10% FBS and 1% penicillin-streptomycin.

Establishment of Cell Model

Glucocorticoids can activate signaling pathways that influence circadian molecular oscillators.[33] They are not only periodically secreted like melatonin, but the glucocorticoid receptor (GR) is ubiquitously expressed in nearly all cells. In addition, its impact on the expression of circadian rhythm genes in tissues is independent of the central SCN pacemaker.[34] Hypoxia is a significant risk factor for the development of AMD, which is caused by age-related changes in retinal barrier structure, leading to deterioration of the supply of nutrients and oxygen to photoreceptors through RPE cells.[35] To simulate AMD, a cellular hypoxia model was created using cobaltous chloride (CoCl2) and synchronized cellular circadian rhythms with dexamethasone (DEX). Because serum shock induces the expression of the circadian rhythm gene in mammalian tissue culture cells,[36] serum-free medium is used to eliminate this effect. We added 100 nM concentration of DEX (MCE, USA) to ARPE-19 cells cultured in serum-free medium for 15 minutes to synchronize the circadian rhythm in the cells. After 48 hours, a serum-free medium containing 200 µM of COCL2 (Sigma-Aldrich, Germany) was replaced. Samples were collected every 4 hours after 60 hours of synchronization, which is served as the circadian rhythm group. Because DEX was dissolved with DMSO (Solarbio, China), the same concentration of DMSO was used to stimulate the control group for 15 minutes. The concentration of JAK2 pathway inhibitor Fedratinib (MCE, USA) was 3 nM.

Enzyme Linked Immunosorbent Assay

The Human VEGFA ELISA kit (Bosterbio, China) was used to detect the VEGFA content in the cell supernatant. The kit was removed from the refrigerator at 4°C and rewarmed at room temperature for 30 minutes. We then collected 100 µL/well of different groups of cell supernatant and added it to the 96-well plate. Then, we sealed it with a sealer film and placed it in a 37 degrees incubator for 1.5 to 2 hours. After the liquid in the plate was completely removed, the prepared biotin-labeled antibody working solution (100 µL/well) was added and incubated in the incubator for 1 hour. Then, we added SA - HRP working solution and incubated it for 0.5 hours. After the liquid was removed, 90 µL TMB of color developing solution was added to each well. Then, we incubated it in the incubator away from light for 7 to 30 minutes and washed off the color developing solution. TMB termination solution (100 µL/well) was added, and the OD values of each group were detected, and the corresponding concentrations were calculated using an enzyme-labeler (Bio-Rad Laboratories, USA).

Cell Counting Kit-8

After cell count and dilution (3000–5000 cells/100 µL), each 100 µL hole was added into the 96-well plate one by one, with 4 pairs of holes in each group. When the cells had grown to about 80%, the drug was added. After the appropriate stimulation time, the cell counting kit-8 (CCK8) reagent (10 µL/well; DOJINDO, Japan) was added and incubated at 37°C for 2 hours. The absorbance of each group was measured at 450 nm using an enzyme-labeler (Bio-Rad Laboratories, USA). The number of surviving cells was calculated using Image J software.

Wound Healing Assay

After the cells grew to 100% confluent in the 6-well plate, a 200 µL pipette tip was used to move vertically across the monolayer cells to produce "wound damage." Then, we removed the cell debris with PBS. After photographing the scratch area for 0 hours, the cells were incubated again using serum-free medium to put the cells in a serum-starved state to exclude proliferation. Images of the same locations were recorded at different points in time to assess the lateral migration ability of the cells. The scratch area was quantified, and the mobility was calculated using ImageJ software.

Transwell Assay

Cells were cultured with serum-free medium for 12 to 24 hours to further remove the influence of serum, and the cells with 70% to 80% confluent degree were digested and then re-suspended with serum-free medium. Then, the count and adjusted cell density was changed to $2.5 * 10^5$/mL. The upper chamber was inoculated with 200 µL cell suspension, and the lower chamber was added with 500 µL medium containing 10% serum. After further culture, it was fixed with 4% PFA and stained with 1% crystal violet (Beyotime, China). Images were taken using microscope (Leica Thunder) and quantified using the ImageJ software.

Endothelial Cell Tube Formation Assay

Matrigel matrix glue (300 µL; BD Biosciences, Canada) was laid flat on a 24-well plate. Cells with a density of $30* 10^4$ were inoculated with 300 µL and the well plates were further incubated in an incubator for 3 to 6 hours. Random images are obtained using a microscope (Leica Thunder). The Angiogenesis analyzer of the ImageJ plug-in was used to

Investigative Ophthalmology & Visual Science

quantify the tube formation ability by counting the number of branches and tubes.

Cellular Immunofluorescence

After the cell slides were placed in 24-well plates, 300 µL of ARPE-19 cell suspension was added to each well. When the cells grew to 70% to 80%, 4% paraformaldehyde was added and fixed at room temperature. Then, the 0.5% Triton X-100 + 5% BSA was closed at room temperature for 2 hours. After incubating the primary antibody at 4 degrees overnight, we incubated the corresponding secondary antibody at room temperature and away from light for 2 hours. The tablets were sealed with anti-fluorescence quenching solution SouthernBiotech (USA) containing DAPI. Images were taken with the Leica Thunder high resolution fluorescence microscope. STRA6 antibody was purchased from Novus (1:200; USA). Fluorescent secondary antibody of goat anti-rabbit was purchased from Abcam (1:200; USA).

EdU Assay for Cell Proliferation

After the cell slides were placed in 24-well plates, 300 µL cell suspension was added to each well. Please refer to the kit instructions for testing. All EdU reagents were obtained from the EDU-594 cell proliferation assay kit (Beyotime, China). The tablets were sealed with anti-fluorescence quenching solution SouthernBiotech (USA) containing DAPI. The images were taken with the Leica Thunder high resolution fluorescence microscope.

Cell siRNA Transfection

Transfection was performed using jetPRIME cell siRNA transfection reagent (Polyplus, France). The cells were inoculated into 6-well plates (10–15 *10^4 cells/well) with 2 mL medium per well. After the cell fusion reached 50%, the siRNA was added to the jetPRIME buffer, immediately swirled for 2 to 3 seconds, and then centrifuged. The vortex was mixed immediately for 2 to 3 seconds and centrifuged. After incubation at room temperature for 10 to 15 minutes, the transfection complex was formed, and the transfection complex was added to the cells containing serum. We gently shook the culture vessel to distribute the transfection compound evenly into the cells. The si-STRA6 and si-NC were synthesized by Generalbio (China). The sequences of the primers used are shown in Supplementary Document S1.

Luciferase Assay

BMAL1 transcription factor (pSE6884), CLOCK transcription factor (pSE7084), STRA6 WT promoter (pSE7565), TK-RLUC (pRL-TK), Promoter vector (pGL3-Basic), Positive control vector (pGL3-Control), and Transcription factor vector (pCDNA3.1) were synthesized and constructed by Sangon Biotech (Shanghai, China). The 293T cells were inoculated into 24-well plates at a confluent rate of 30% to 50%, with 3 compound pores in each group. The target and control plasmids were transfected 12 to 20 hours later. Preparation of DNA and transfection reagents: when transfecting plasmid with 24-well plates, the ratio per well is DNA: transfection reagent = 320 ng: 3 µL; Transcription factor: promoter: TK-RLUC = 75 ng: 225 ng: 20 ng. The mixture and transfection reagent were diluted, respectively, and incubated at room temperature for 5 minutes. The diluted mixture was mixed with the transfection reagent, incubated at room temperature for 20 minutes, and then added to the cell sample. Then, 6 hours after transfection, the fluid was changed. At 48 hours after the transfection, the medium was discarded and washed once with 1 × PBS. The 24-well plate was tilted and drained of the remaining PBS. Then, 1 × PLB was prepared and stored at 4°C before use. We then added 200 µL diluted 1 × PLB to each well and shook at 4°C for 15 minutes in a shaker for cracking. Then, we placed a white, light-tight 96-well plate on ice and added 20 µL pre-mixed LAR II to each hole. The cracked cells and PLB were blown and sucked repeatedly and added into the pore plate. Then, 29 µL of PBS was added to each hole, and the supernatant of the cell lysate was 1 µL. Luciferase activity was detected by enzymoscope (Tecan, Switzerland) after 2 seconds. Then, immediately we added 20 µL pre-mixed Stop & Glo Reagent to each hole, and test data after left standing still for 2 seconds. We then divided the data from Firefly luciferase by the data from Renialla luciferase and plot it with Image J software (National Institutes of Health, USA). The Dual-Luciferase Reporter Assay System was purchased from Promega (USA). The carrier synthesis report is located in Supplementary Document S3.

Transcriptome Sequencing and Bioinformatics Analysis

We extracted RPE-choroid-scleral complex tissues from two groups of mouse eyeballs for full transcriptome sequencing. The sequencing data have been deposited in the NCBI Gene Expression Omnibus (GEO; https://www.ncbi.nlm.nih.gov/geo/) database under the accession code GSE253949. The differential expression of messenger RNAs (DEmRNAs) between the two group samples was identified using the "limma" package. Using the limma R package, we identified differentially expressed genes (DEGs) between 2 risk groups according to the following conditions: $\log2|FC|>1$, an adjusted P value < 0.05 and a false discovery rate (FDR) < 0.05. In addition, we conducted differential expression gene analysis and GSVA enrichment analysis on the public dataset GSE29801 ($n = 293$). Using the "GSVA" R package, the related pathways of gene enrichment were identified.

Protein-Protein Interaction

Based on STRA6, all proteins that have direct interactions were obtained using the Search Tool for the Retrieval of Interacting Genes Database (STRING; https://cn.string-db.org/). These interactions produce non-directed edges between protein nodes. The protein–protein interaction (PPI) networks were constructed and visualized by Cytoscape 3.9.0.

Prediction of Transcription Factor Binding Sites

Calculate STRA6 promoter regions (Chr15: 74212160–74214259) through the NCBI database (https://www.ncbi.nlm.nih.gov/). CLOCK was selected as the transcription factor in the JASPAR database (https://jaspar.elixir.no/) and the STRA6 promoter region sequence was copied to "Scan." We then set the relative score threshold to 90%. The binding sites were screened according to the score. We used WebLogo (https://weblogo.threeplusone.com/create.cgi) to draw images. Promoter sequences and possible binding sites are in Supplementary Document S2.

Investigative Ophthalmology & Visual Science

Statistical Analysis

In this study, all statistical analyses were performed using R software (version 4.1.2; https://www.r-project.org/) and GraphPad Prism software (version 9.5.1). Analysis of variance and Student's *t*-test were used for comparison between groups. All values were expressed as mean ± SEM. Any P value < 0.05 was considered statistically significant.

Results

Circadian Rhythm Disturbance Promotes CNV in Mouse Model

Mice models of circadian rhythm and jet lag were constructed, as illustrated in Figure 1A. The abnormal blood flow signals at the laser site confirmed neovascularization, thus validating the successful establishment of the laser model (Fig. 1B). The transcription factor BMAL1 and CLOCK are central components of the mammalian biological clock, and serve as its primary driver.[33] We confirmed the successful induction of circadian disturbance by detecting abnormal oscillatory expression of BMAL1 and CLOCK (Figs. 1C–F). As shown in Figure 1G, fundus leakage was most pronounced on the seventh day post laser. Consequently, the seventh day was chosen to investigate the impact of circadian rhythm disturbance on CNV formation. The H&E staining and CD31 immunofluorescence indicated a significant increase in CNV size in mice with jet lag compared to those with normal circadian rhythm (Figs. 1H–K).

The Expression of STRA6 is Upregulated in Circadian Rhythm Disturbance and CNV

Further, we performed full transcriptome sequencing (Fig. 2A). Subsequent analysis revealed 290 genes with increased expression and 425 genes with decreased expres-

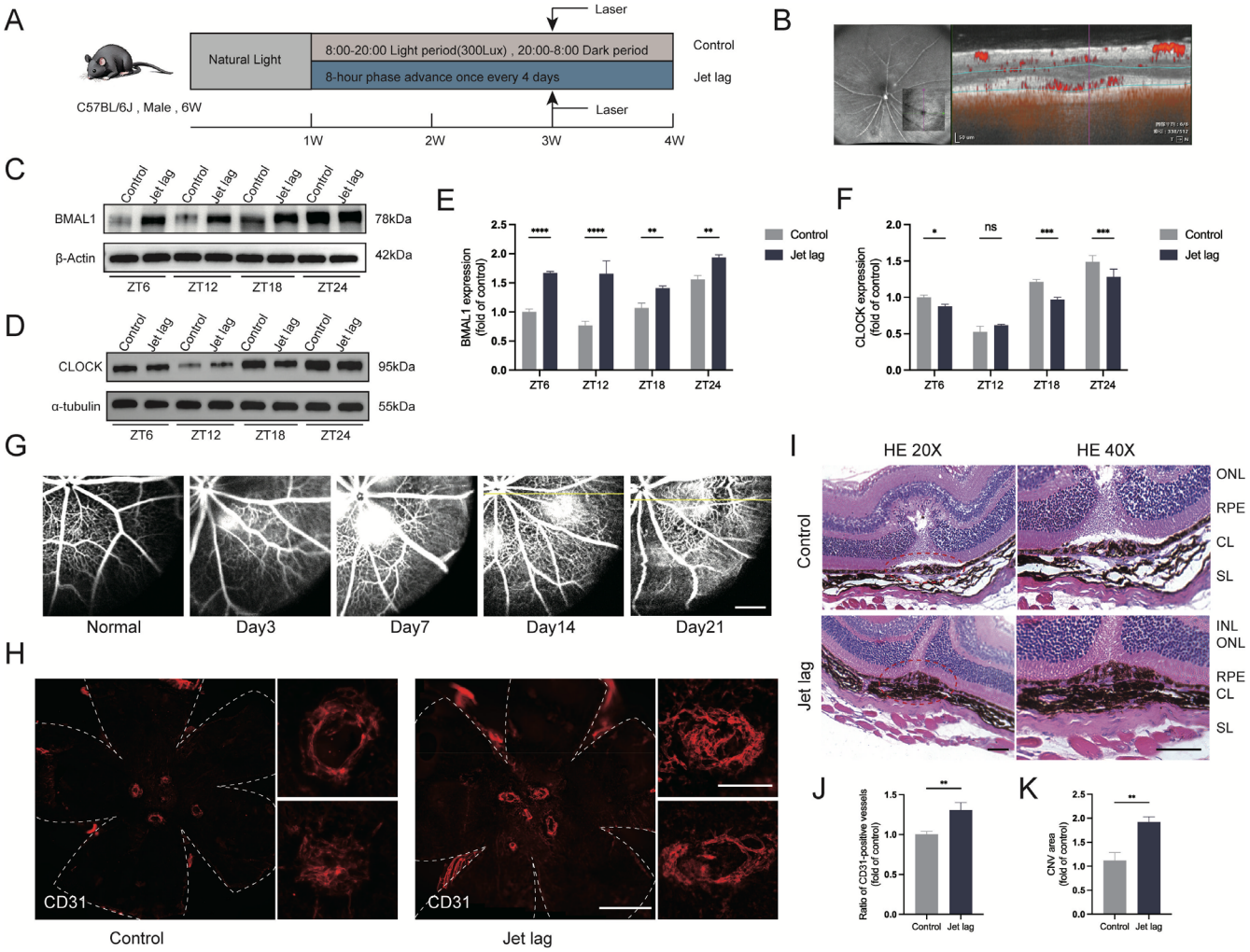

Figure 1. Establishment of animal model of jet lag and its influence on CNV formation. (**A**) Schematic diagram of mouse circadian rhythm disturbance combined with laser-induced CNV model construction. (B) Fundus OCTA of mice on day 7 after laser (scale = 50 µm). (**C** to **F**) Expression of clock gene BMAL1 and CLOCK in mouse RPE-choroid-sclera complex ($n = 5$ mice at each time point/group). (**G**) FFA images of mouse CNV model induced by laser at different time points ($n = 3$/group, scale = 100 µm). (**H** and **J**) CD31 immunofluorescence of mouse eye choroidal film ($n = 3$/group, scale = 1000 µm and 100 µm). (**I** and **K**) H&E staining was performed on the section of mouse eye lesions ($n = 3$/group, scale = 100 µm). CL, choroid layer; INL, inner core layer; ONL, outer nuclear layer; RPE, retinal pigment epithelium; SL, sclera layer; ZT, zeitgeber time; error bars represent mean ± SEM; *ns* was not statistically significant; $^{*}P < 0.05$, $^{**}P < 0.01$, $^{***}P < 0.001$, and $^{****}P < 0.0001$.

Investigative Ophthalmology & Visual Science

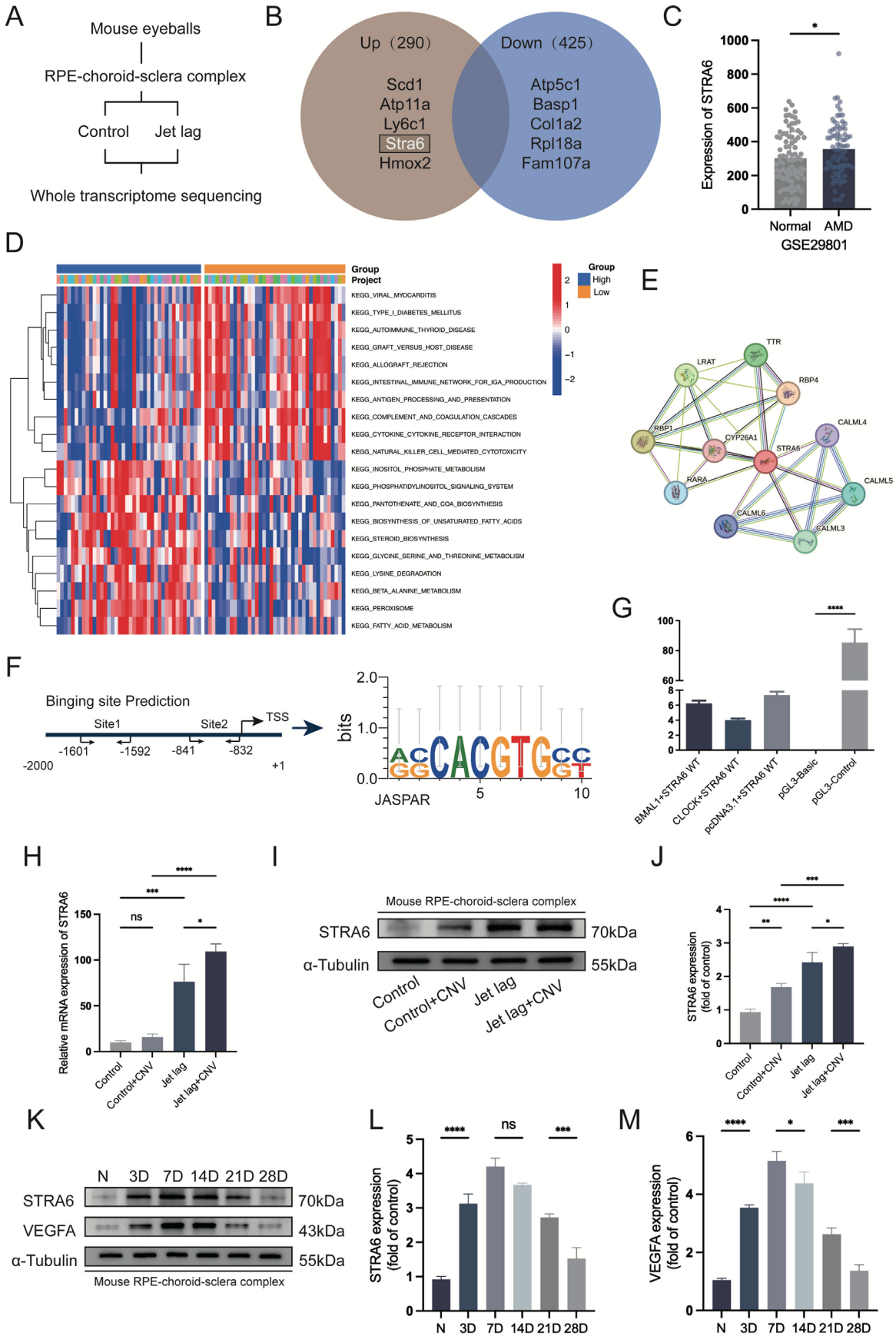

Figure 2. Correlation analysis of STRA6 and the influence of circadian rhythm and CNV on it. (**A**) Schematic diagram of complete transcriptome sequencing in mouse tissue. (**B**) Venn diagram of mRNA upregulation and downregulation in sequencing results. (**C**) Analysis

of STRA6 gene expression differences in public dataset GSE29801 (n = 293). (**D**) Heat map of GSVA analysis in patients with AMD with high and low STRA6 expression. (**E**) STRA6 protein-protein interaction. (**F**) A possible binding site to the CLOCK gene. (**G**) Luciferase assay showed the regulatory effects of BMAL1 and CLOCK on STRA6. (**H**) The expression of STRA6 mRNA in each group was detected by qRT-PCR (n = 3 independent experiment). (**I** and **J**) STRA6 protein expression levels in each group (n = 3 independent experiments). (**K** to **M**) The expression of STRA6 and VEGFA protein in RPE-choroid-sclera complex in CNV model mice induced by laser at different time points (n = 3 independent experiments). ZT, zeitgeber time; error bars represent mean ± SEM; *ns* was not statistically significant; $^{*}P < 0.05$, $^{**}P < 0.01$, $^{***}P < 0.001$, and $^{****}P < 0.0001$.

sion in the disturbed group. Notably, genes such as SCD1, ATP11A, LY6C1, STRA6, and HMOX2, exhibited significant differences in expression levels among those with increased expression, whereas ATP5C1, BASP1, COL1A2, RPL18A, and FAM107A showed prominent differences among those with decreased expression (Fig. 2B). STRA6 was selected for follow-up experiments based on its related research on circadian rhythm and neovascularization. Analysis of the public dataset GSE29801 (n = 293) indicated that STRA6 was expressed at higher levels in patients with AMD compared to the control group (Fig. 2C). GSVA revealed that patients with AMD with high or low STRA6 expression were differentially enriched in the pathways that promote angiogenesis, including inositol phosphate metabolism, the phosphatidyl inositol signaling system (PI3K/AKT),[37] pantothenic acid, and Coenzyme A biosynthesis,[38] etc. (Fig. 2D). PPI indicated interactions of STRA6 with CYP26A1, CALML3, TTR, etc. (Fig. 2E). Finally, we analyzed the sequence characteristics of STRA6 promoter, and identified the possible binding sites to the CLOCK gene through the JASPAR database (Fig. 2F). In addition, we confirmed the regulatory effects of BMAL1 and CLOCK on STRA6 by Luciferase Assay (Fig. 2G). These analyses provide valuable insights for further mechanism-related research.

To verify the accuracy of the sequencing results, RT-qPCR and Western blotting (WB) were used to assess STRA6 expression levels in different groups of mice. The findings revealed a significant upregulation of STRA6 expression in the jet lag group, with laser-induced CNV formation further enhancing this expression (Figs. 2H–J). To investigate the correlation between STRA6 and VEGF and determine the optimal time point for subsequent studies, we examined the expression of proteins on days 3, 7, 14, 21, and 28. We found that both had a similar expression trend, increasing gradually in the early stage, reaching a peak value on the seventh day after laser, and then gradually decreasing. This finding suggests that there may be some association between them, and that the 7-day time point was chosen due to the highest expression (Figs. 2K–M).

The Knockdown of STRA6 Inhibits the Promotion of CNV Formation In Vivo by Jet Lag

To investigate the impact of STRA6 on CNV in vivo, siSTRA6 was injected into the vitreous cavity of C57BL/6J mice for a 2-week period, with siNC serving as the control. Three distinct siRNAs were designed to knock down STRA6 levels in the mouse RPE-choroid-sclera complex. RT-qPCR and WB illustrated that all three siRNAs effectively decreased the protein expression of STRA6 (Figs. 3A–C). siRNA #1 was selected for subsequent experiments due to its superior knockdown efficiency. Subsequent verification confirmed the significant reduction in STRA6 levels following siSTRA6 injection (Fig. 3D). Immunofluorescence analysis of IB4 choroidal flat-mount revealed an increase in neovascularization after circadian rhythm disturbance, which was reversed upon STRA6 knockdown (Figs. 3E, 3F). These findings suggest an important role for STRA6 in pathological angiogenesis under conditions of disrupted circadian rhythms. The H&E staining demonstrated that STRA6 knockdown led to reduced neovascularization (Figs. 3G, 3H). Additionally, OCTA indicated a certain extent of reduction in neovascularization thickness, area, and abnormal blood flow under jet lag conditions following STRA6 knockdown (Figs. 3I–L). Collectively, these results indicate that STRA6 knockdown mitigates CNV formation promoted by circadian disturbance in vivo.

STRA6 Influenced ARPE-19 Cell Proliferation, Migration, and VEGF Secretion in the Case of Unsynchronized Circadian Rhythms

We carried out in vitro studies through cell experiments. Immunofluorescence staining of APRE-19 revealed significant nuclear expression of STRA6 (Fig. 4A). Subsequently, we established a model of cellular circadian rhythm combined with hypoxia. The optimal concentrations were determined through CCK8 screening (Figs. 4B, 4C), and COCL2 was selected at a concentration of 200 µM (µmol/L). Combining our own results and its use in other literature, we chose a concentration of 100 nM (nmol/L) for subsequent experiments. The construction of the model is illustrated in Figure 4D. The clock gene BMAL1 and CLOCK were used to demonstrate the effectiveness of modeling (Figs. 4E–H).

In the following study, the expression of STRA6 in ARPE-19 cells was reduced through transfection of siRNA, with siSTRA6 #3 demonstrating the highest knockdown efficiency (Figs. 4I, 4J). The effectiveness of knockdown was confirmed by WB analysis in Figure 4K. Transwell and wound healing assays indicated a decrease in the migration ability of ARPE-19 cells after circadian rhythm synchronization, with a similar effect observed in cells without circadian rhythm upon STRA6 knockdown (Figs. 4L–Q). The proliferation experiment of CCK-8 in Figure 4R showed that cells with unsynchronized circadian rhythm had strong proliferation ability, which was effectively inhibited by STRA6 knockdown. ELISA demonstrated a decrease in VEGF secretion in the cell supernatant post-circadian rhythm synchronization, which further decreased following STRA6 knockdown. Interestingly, non-rhythmic cells exhibited a more significant inhibition of VEGF secretion after STRA6 knockdown compared to cells with synchronized circadian rhythm (Fig. 4S). These findings suggest that STRA6 knockdown leads to reduced proliferation and migration of unsynchronized RPE cells, along with decreased VEGF secretion.

KnockDown STRA6 Inhibits Endothelial Cells Multiplication, Migration, and Tube Formation

Pathologically elevated VEGF promotes the pathological growth of endothelial cells, leading to CNV. We collected the

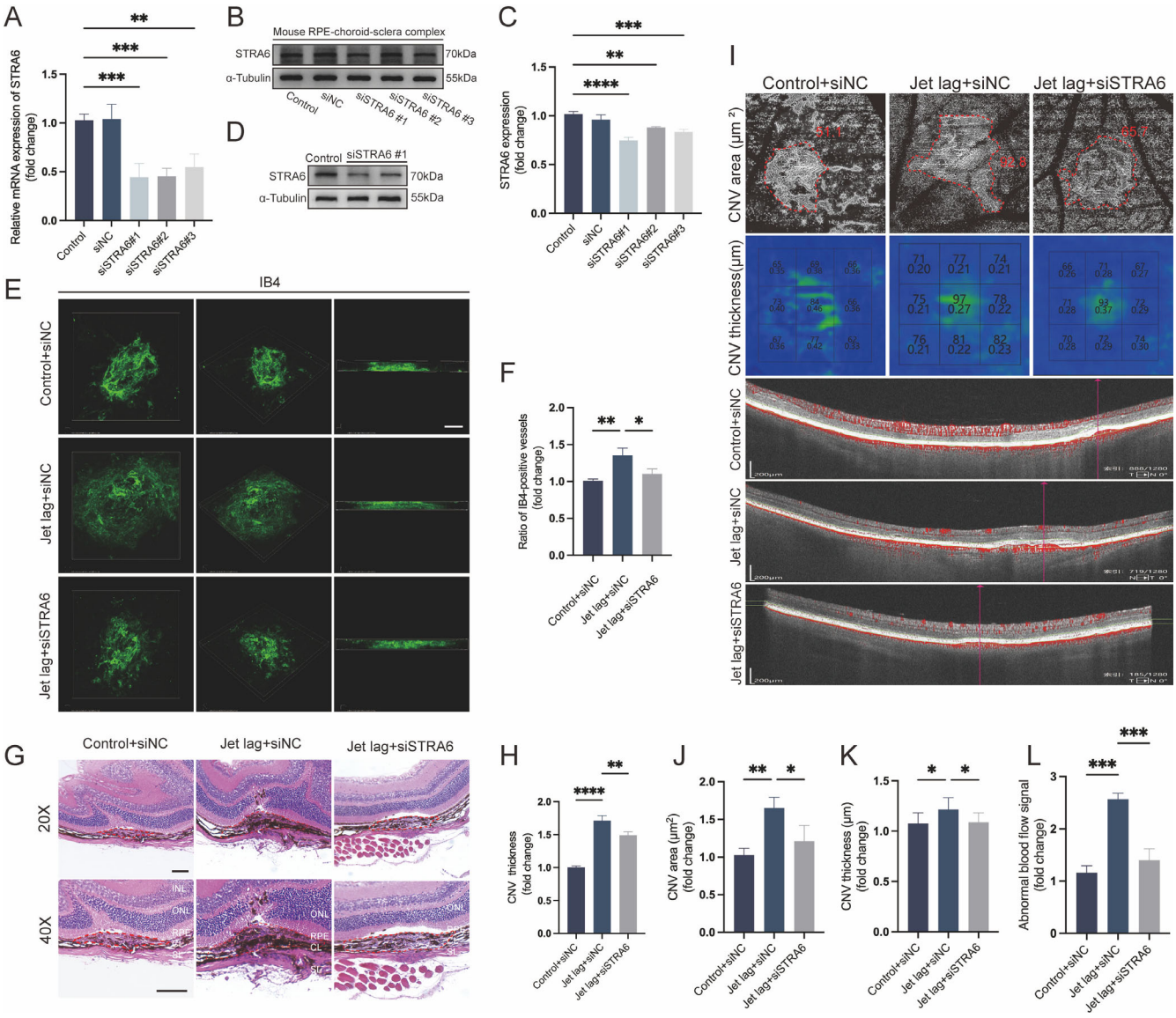

Figure 3. Effects of STRA6 knockdown on CNV formation in vivo. (**A**) The expression of STRA6 mRNA in each group was detected by qRT-PCR ($n = 3$ independent experiment). (**B** and **C**) STRA6 protein expression levels in each group ($n = 3$ independent experiments). (**D**) STRA6 knockdown verification ($n = 3$ independent experiments). (**E** and **F**) The scale of neovascularization was shown by IB4 immunofluorescence in mouse choroid ($n = 3$/group, scale = 100 μm). (**G** and **H**) H&E staining was performed on slices of diseased eye area of mice ($n = 3$/group). CL, choroid layer; INL, inner core layer; ONL, outer nuclear layer; RPE, retinal pigment epithelium; SL, sclera layer; scale = 100 μm). (**I** to **L**) OCTA showed the thickness, area, and blood flow of new vessels in each group ($n = 3$/group, scale = 200 μm). ZT, zeitgeber time; error bars represent mean ± SEM; *ns* was not statistically significant; $^{*}P < 0.05$, $^{**}P < 0.01$, $^{***}P < 0.001$, and $^{****}P < 0.0001$.

supernatant of ARPE-19 cells from each group and cultured HUVECs and RF/6A cells. Transwell and wound healing assays revealed that under hypoxia conditions, the ARPE-19 cell supernatant reduced the migration capacity of endothelial cells compared to the control group when synchronized with the circadian rhythm, with similar effects observed after STRA6 knockdown (Figs. 5A–E, Figs. 6A–E). In the tube formation assay, both synchronized circadian rhythm and ARPE-19 supernatant treated with siSTRA6 significantly reduced the cumulative number of tubular structures formed by HUVECs and RF/6A cells (Figs. 5F–H, Figs. 6F–H). EdU proliferation assay results demonstrated that culturing with ARPE-19 supernatant post-STRA6 knockdown effectively alleviated the problem of enhanced proliferation ability of HUVECs and RF/6A cells caused by unsynchronized cell supernatant (Figs. 5I, 5J, Figs. 6I, 6J). These findings provide evidence for the role of STRA6 knockdown in inhibiting angiogenesis in the context of circadian rhythm disturbance.

STRA6 is Involved in Inflammation and is Associated With VEGF

Immunofluorescence staining was performed on mouse eyeballs 7 days post-laser injury using markers for macrophages (F4/80), endothelial cells (IB4), and STRA6. The results revealed significant enrichment of STRA6 in the lesions, showing high colocalization with macrophages, which were concentrated around the laser injury sites. In addition, STRA6 is expressed internally in choroidal

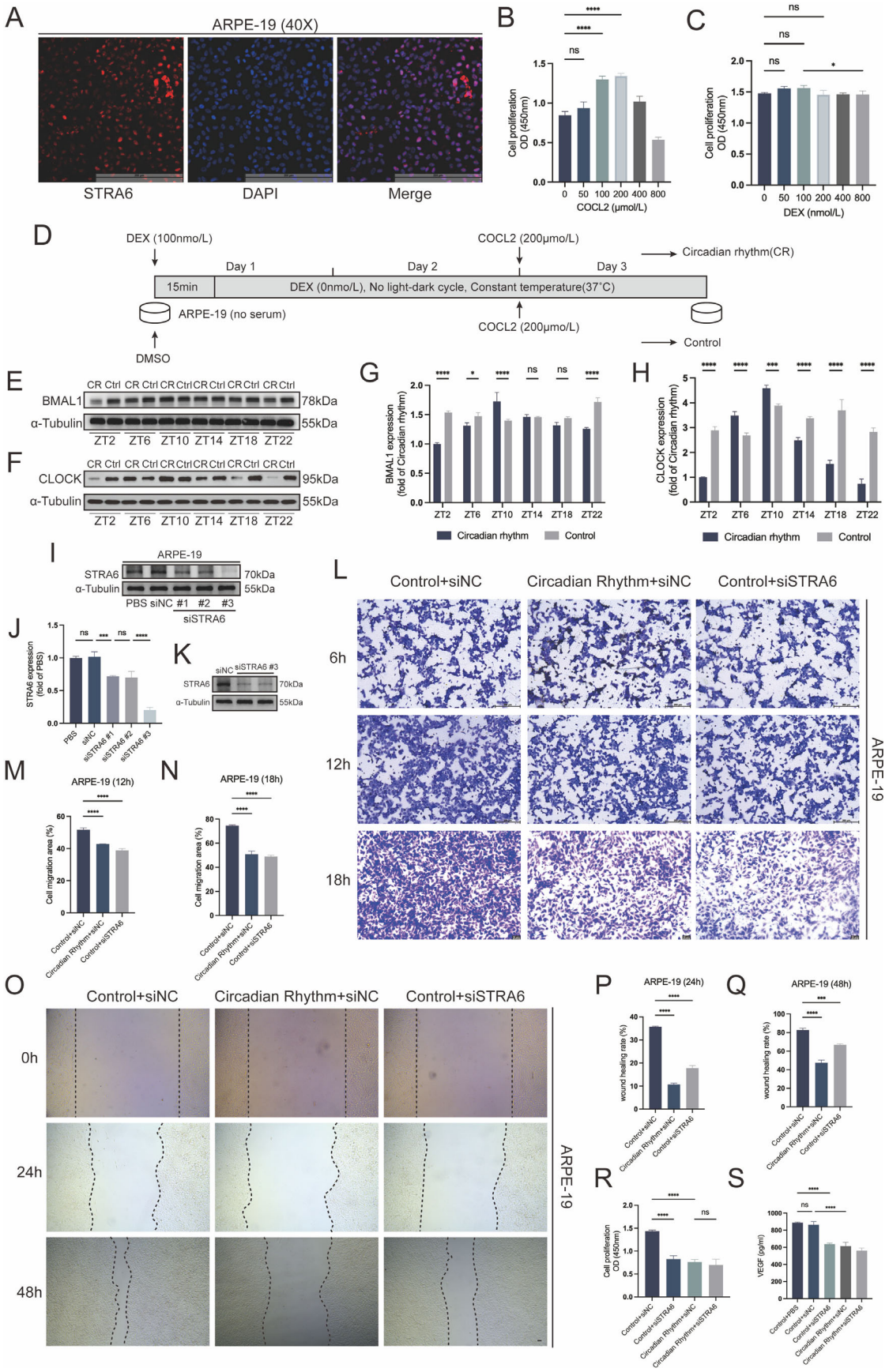

Figure 4. Construction of circadian rhythm cell model and effect of STRA6 knockdown on RPE cell function in vitro. (**A**) Immunofluorescence staining of ARPE-19 cells ($n = 3$ independent experiments; *red* = STRA6, *blue* = DAPI; scale = 200 μm). (**B**) The effects of different

concentrations of COCL2 on the proliferation of ARPE-19 cells were detected by CCK8 (μmol/L; $n = 3$ independent experiments). (**C**) The effects of different concentrations of DEX on the proliferation of ARPE-19 cells was detected by CCK8 (nmol/L; $n = 3$ independent experiments). (**D**) Schematic diagram of cell synchronization circadian rhythm model construction. (**E** to **H**) Expression of clock gene BMAL1 and CLOCK protein in ARPE-19 cells in each group ($n = 3$ independent experiments). (**I** and **J**) STRA6 protein expression levels in each group ($n = 3$ independent experiments). (**K**) STRA6 knockdown verification ($n = 3$ independent experiments). (**L** to **N**) Transwell showed the migration of ARPE-19 cells ($n = 3$ independent experiments; scale = 6–12 hours 200 μm, 8 hours 50 μm). (**O** to **Q**) The wound healing assay showed the migration of ARPE-19 cells in each group at 24 hours and 48 hours ($n = 3$ independent experiments; scale = 50 μm). (**R**) The proliferation of ARPE-19 cells in each group was detected by CCK8 ($n = 3$ independent experiments). (**S**) VEGF in cell supernatant was detected by ELISA ($n = 3$ independent experiments). ZT, zeitgeber time; error bars represent mean ± SEM; *ns* was not statistically significant; $^{*}P < 0.05$, $^{**}P < 0.01$, $^{***}P < 0.001$, and $^{****}P < 0.0001$.

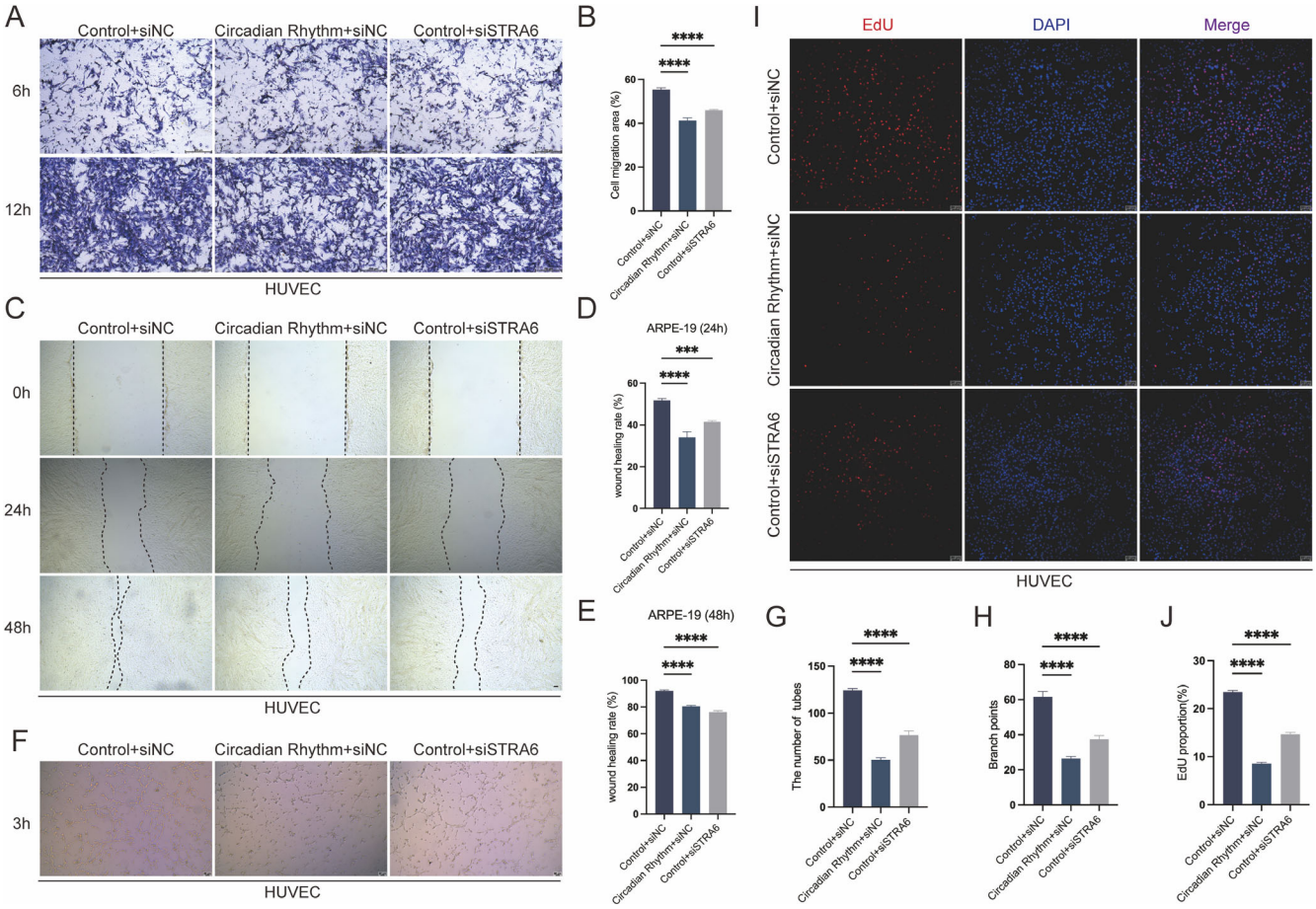

Figure 5. Effect of RPE cell supernatant on endothelial cell proliferation and migration tube formation under different conditions. (**A** and **B**) Transwell assay showed the effect of ARPE-19 cell supernatant on HUVEC migration at 6 hours ($n = 3$ independent experiments, scale = 200 μm). (**C** to **E**) The effect of supernatant of ARPE-19 cells on the migration ability of HUVECs at 24 hours and 48 hours was demonstrated by wound healing assay ($n = 3$ independent experiments; scale = 50 μm). (**F** to **H**) The effect of the supernatant of ARPE-19 cells on the formation of HUVECs tubes was detected by endothelial cell tube formation experiment ($n = 3$ independent experiments; scale = 50 μm). (**I** and **J**) EdU proliferation assay was used to detect the effect of ARPE-19 cell supernatant on the proliferation of HUVECs ($n = 3$ independent experiments; scale = 50 μm). ZT, zeitgeber time; error bars represent mean ± SEM; *ns* was not statistically significant; $^{*}P < 0.05$, $^{**}P < 0.01$, $^{***}P < 0.001$, and $^{****}P < 0.0001$.

vessels, which is consistent with its role in blood interaction with RBP (Fig. 7A).[39] Circadian fluctuations in VEGFA protein levels were observed in ARPE-19 cells after circadian synchronization in both normal and hypoxic groups. Peak expression occurred around noon, whereas the lowest expression was observed around midnight. The difference was that unsynchronized circadian rhythms led to a physiological decrease in overall VEGFA expression in normal ARPE-19 cells and a pathological increase in expression in hypoxic ARPE-19 cells (Figs. 7B–E). This suggests that both VEGFA and STRA6 are pathologically elevated following circadian rhythm disturbance. To explore the relationship between VEGFA and STRA6, we also examined the rhythm of STRA6. The results showed that STRA6 expression peaking around noon and dropping at midnight, which is similar to VEGFA, suggesting the potential correlation between the two proteins (Figs. 7F, 7G).

STRA6 Promotes CNV Formation by Activating JAK2/STAT3/VEGFA Signaling in RPE Cells

Next, we studied the expression levels of pathway-related molecules, revealing that both JAK2 and STAT3 exhibited a circadian expression trend like STRA6 and VEGFA

Investigative Ophthalmology & Visual Science

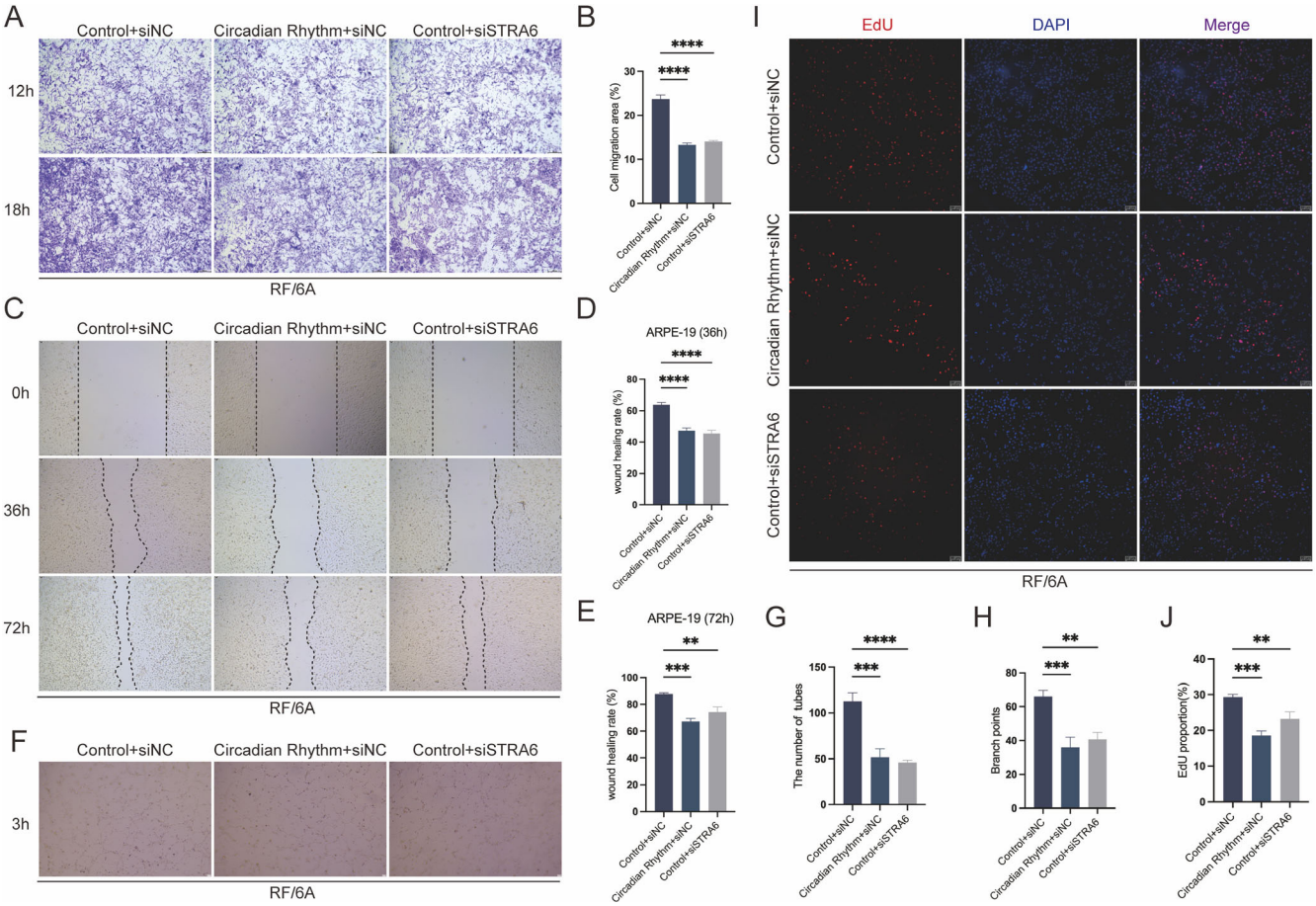

Figure 6. Effect of RPE cell supernatant on endothelial cell proliferation and migration tube formation under different conditions. (**A** and **B**) Transwell assay showed the effect of ARPE-19 cell supernatant on RF/6A cell migration ($n = 3$ independent experiments; scale = 200 µm). (**C** to **E**) The effect of supernatant of ARPE-19 cells on the migration ability of RF/6A cells at 36 hours and 72 hours was demonstrated by wound healing assay ($n = 3$ independent experiments; scale = 50 µm). (**F** to **H**) The effect of the supernatant of ARPE-19 cells on the formation of RF/6A tubes was detected by endothelial cell tube formation experiment ($n = 3$ independent experiments; scale = 200 µm). (**I** and **J**) EdU proliferation assay was used to detect the effect of ARPE-19 cell supernatant on the proliferation of RF/6A cells ($n = 3$ independent experiments; scale = 50 µm). ZT, zeitgeber time; error bars represent mean ± SEM; *ns* was not statistically significant; $^{*}P < 0.05$, $^{**}P < 0.01$, $^{***}P < 0.001$, and $^{****}P < 0.0001$.

(Figs. 8A–D). Phosphorylated JAK2 and STAT3, as well as VEGFA protein expressions, were observed to increase when the circadian rhythm was unsynchronized and decrease when STRA6 was knocked down (Figs. 8E, 8F). To further investigate the impact of JAK2/STAT3 signal transduction on VEGFA, we treated unsynchronized ARPE-19 cells with the JAK2 inhibitor fedratinib and COCL2. As anticipated, in an anoxic cell model with unsynchronized rhythms, the inhibition of JAK2/STAT3 activation by fedratinib led to a corresponding downregulation of VEGFA (Figs. 8G, 8H). Above all, these findings suggest that STRA6 contributes to promoting CNV formation by activating JAK2/STAT3/VEGFA signaling in RPE cells.

Discussion

Light serves as the key factor in synchronizing the suprachiasmatic nucleus (SCN), the central pacemaker of the circadian rhythm, with the daily cycle.[40] In mammals, circadian rhythms are generated primarily by retinal perception of light signals transmitted directly through the retinohypothalamic tract to the SCN, which contains the circadian rhythm master pacemaker, to regulate circadian rhythms throughout the body.[41] Interestingly, the circadian rhythm of the mammalian retina operates independently from the central SCN clock. This retinal circadian rhythm system plays a crucial role in a range of physiological functions of the eye, such as visual processing, changes in corneal thickness and eye pressure, disc detachment and phagocytosis, and susceptibility to light-induced photoreceptor damage.[42] Previous research has demonstrated the significant impact of circadian rhythm disruption on various eye diseases, including dry eye, glaucoma, cataract, myopia, and diabetic retinopathy.[40] Wet AMD, characterized by CNV and subretinal neovascularization fibrous tissue, is responsible for 80% of the vision loss of patients with AMD.[43] Studies have indicated that circadian rhythm plays a role in the occurrence and development of pathological angiogenesis, with a subset of genes in vascular endothelial cells exhibiting a 24-hour rhythm of gene expression cycle.[44] Melatonin, a hormone responsible for regulating circadian and seasonal rhythms, has been shown to inhibit the formation of CNV.[45–47] Despite this, the specific impact of circadian rhythm on CNV has not been thoroughly investigated. Through our mouse and cellu-

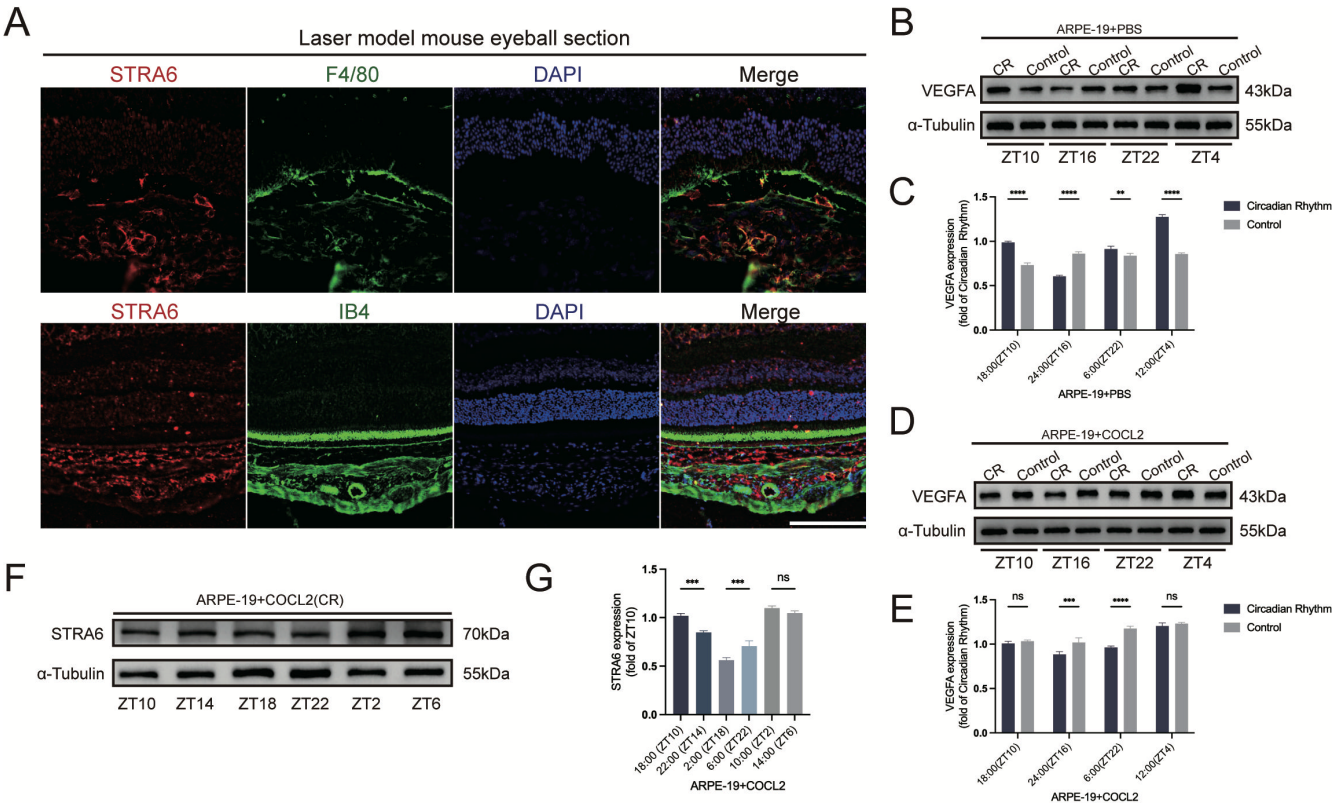

Figure 7. Relationship between STRA6 and inflammation and VEGF. (**A**) Laser induced immunofluorescence staining of paraffin sections of CNV model mice ($n = 3$/group; *red* = STRA6; *green* = F4/80, IB4; *blue* = DAPI; scale = 100 µm). (**B** and **C**) Expression of VEGFA protein in ARPE-19 cells at different time points in the non-combined hypoxia model ($n = 3$ independent experiments). (**D** and **E**) Expression of VEGFA protein in ARPE-19 cells at different time points in the non-combined hypoxia model ($n = 3$ independent experiments). (**F** and **G**) STRA6 protein expression in ARPE-19 cells at different time points after circadian rhythm synchronization in the combined hypoxia model ($n = 3$ independent experiments). ZT, zeitgeber time; error bars represent mean ± SEM; *ns* was not statistically significant; $^{*}P < 0.05$, $^{**}P < 0.01$, $^{***}P < 0.001$, and $^{****}P < 0.0001$.

lar circadian rhythm models, we have successfully demonstrated the exacerbating effect of circadian rhythm disruption on CNV formation both in vivo and in vitro, suggesting that circadian disruption may be an important risk factor for AMD.

The transcription factor BMAL1 is a major driver of mammalian molecular clocks.[33] BMAL1 signaling is involved in promoting neovascularization, and its deficiency results in a significant decrease in new blood vessel formation. Studies have demonstrated that the deletion of other clock genes, such as CLOCK, also inhibits abnormal and excessive blood vessel growth.[48] Disruption of the circadian rhythm leads to a pathological increase in BMAL1 levels, which contributes to heightened angiogenesis, as supported by our findings in this paper. The expression of BMAL1 protein is notably elevated in animal and cell models with circadian rhythm disturbances and desynchronized rhythms, indicating that circadian rhythm disruptions upregulate BMAL1 expression in tissues, thereby fostering the occurrence and development of pathological angiogenesis. VEGF plays a crucial role in angiogenesis, with the RPE layer serving as a major source of this protein and exhibiting circadian rhythms. Research indicates that VEGF expression follows a circadian pattern.[16] Actually, VEGF is a direct transcriptional target of the clock gene BMAL1 and is primarily involved in developmental angiogenesis regulated by the circadian clock.[49] This study observed a circadian rhythm in VEGF expression in RPE cells, noting an increase during pathological conditions and a decrease during physiological conditions after the circadian rhythm is disturbed. This fluctuation may be linked to VEGF's protective function in the retina, safeguarding retinal neurons, RPE, and endothelial cells while supporting the fenestration of choroidal endothelial cells for optimal nutrient supply to photoreceptors.[50] Furthermore, our findings revealed a close similarity between the circadian protein expression patterns of VEGF and BMAL1. These results suggest that BMAL1 is an important factor affecting the occurrence and development of CNV after circadian rhythm disturbance.

Given the exclusive expression of the eye clock gene in photoreceptor cells and the significant influence of light, we hypothesize that the eye circadian rhythm is controlled by cone photoreceptors. Vitamin A, a key component of the photoconductive cycle of vertebrate retinas, plays a vital role in light reception and visual perception.[51] Absorbed through the small intestine, it is converted into all-trans retinol within intestinal cells. All-trans retinol enters cells via the blood stream bound to retinol-binding protein 4 (RBP4) with the help of transmembrane transporters, stimulated by STRA6. As a multi-transmembrane domain protein, STRA6 was identified as an RBP-specific membrane receptor in bovine RPE cells in 2007, and was found to bind to RBP with high affinity and have strong vitamin A-RBP complex uptake activity. It is widely expressed in both embryonic development and adult

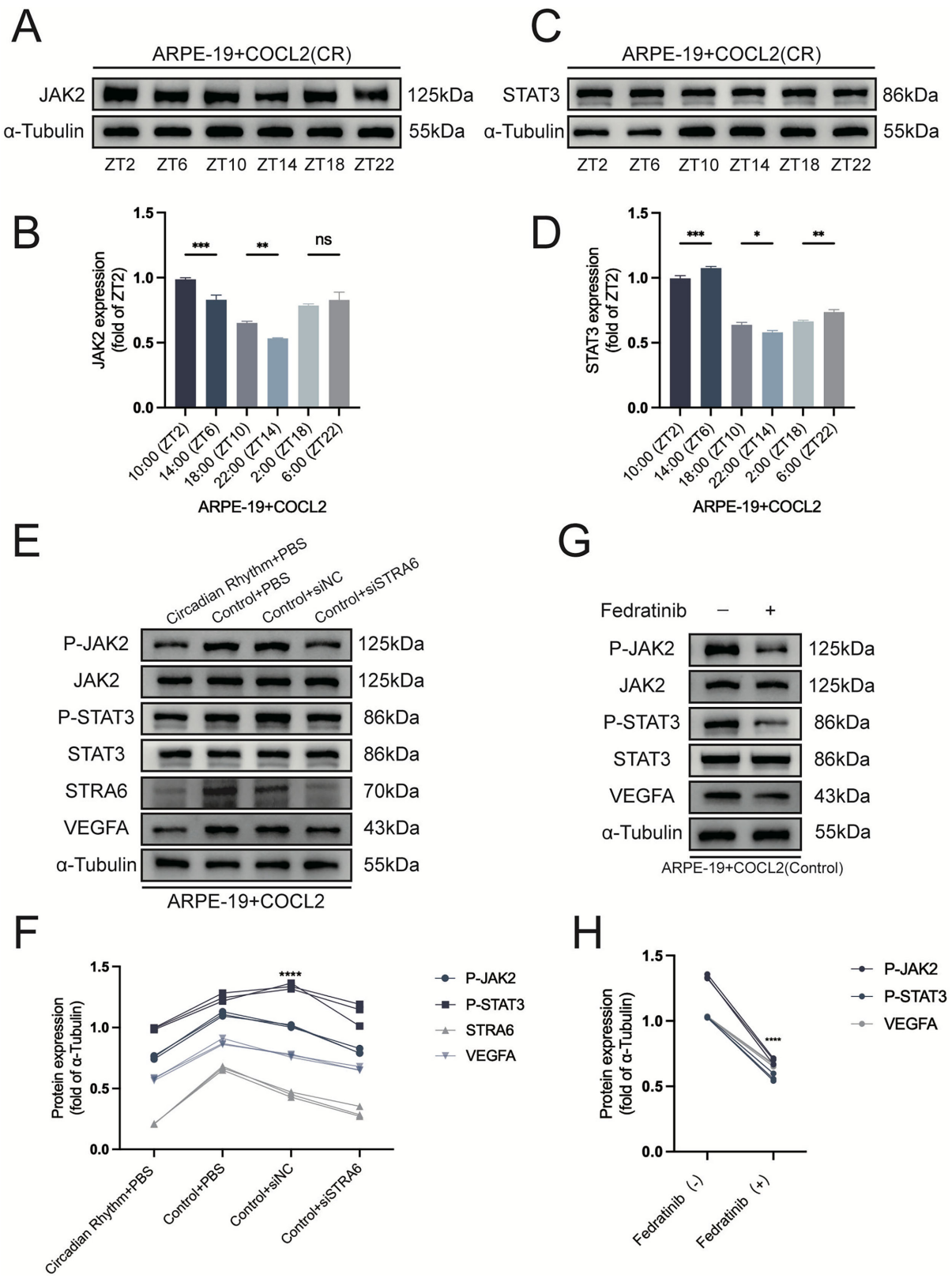

Figure 8. Effect of STRA6 on CNV formation by activating JAK2/STAT3/VEGFA signaling in RPE cells. (**A** and **B**) The expression of JAK2 protein in circadian rhythm ($n = 3$ independent experiments). (**C** and **D**) The expression of STAT3 protein in circadian rhythm ($n = 3$ independent experiments). (**E** and **F**) Expression of P-JAK2, JAK2, P-STAT3, STAT3, STRA6, and VEGFA in ARPE-19 cells of each group ($n = 3$ independent experiments). (**G** and **H**) Expression of P-JAK2, JAK2, P-STAT3, STAT3, and VEGFA proteins in ARPE-19 cells that did not synchronize circadian rhythm after addition of JAK2 pathway inhibitors ($n = 3$ independent experiments). ZT, zeitgeber time; error bars represent mean ± SEM; *ns* was not statistically significant; $^{*}P < 0.05$, $^{**}P < 0.01$, $^{***}P < 0.001$, and $^{****}P < 0.0001$.

organ systems, serving as the main physiological medium for cellular vitamin A uptake.[17] Previous research indicates the presence of STRA6 on choroidal and macrophage cells, a finding corroborated by our own experiment.[52] Notably, vitamin A consumption has been linked to a reduced risk of AMD, and supplementation of STRA6 can enhance vitamin A uptake under normal physiological conditions.[53] Sequencing data reveal a significant increase in STRA6 levels following disturbances in circadian rhythm. This elevation in STRA6 expression may result in excessive vitamin A intake, leading to an increase in the pro-angiogenic factor all-trans retinol, a potential risk factor for exudative AMD.[24] Our results suggest that STRA6 knockdown can effectively mitigate the CNV promotion effect of circadian rhythm disturbance in mice and cell models.

Chronic inflammation is a key factor in numerous human diseases, with morbidity and mortality frequently linked to metabolic dysfunction. Inflammation and metabolic processes vary with circadian timing, suggesting important temporal crosstalk between these systems. However, the connection between these processes in eye diseases has not been thoroughly explored. This research reveals that STRA6, a protein closely tied to metabolism, is recruited in macrophages, and influences pathological angiogenesis through the inflammatory pathway involving JAK2/STAT3. These findings suggest that investigating the role of STRA6 could serve as a valuable starting point for delving into the intersection of ocular inflammation and metabolism.

This study represents the first attempt to establish a connection between circadian rhythms and AMD. By developing an animal model, the researchers were able to show that disruptions in circadian rhythms can lead to pathological angiogenesis. Following the successful validation of the model, a comprehensive transcriptome sequencing was conducted to identify differentially expressed genes, with a focus on STRA6 for further investigation. The findings revealed a circadian rhythm of JAK2/STAT3 in the mouse eye, with evidence suggesting that STRA6 promotes CNV formation by activating the JAK2/STAT3/VEGFA signaling pathway in RPE cells. This study sheds light on the significance of circadian rhythms in neovascularization associated with AMD, offering potential new avenues and targets for anti-VEGF therapy.

Conclusions

This study suggests that STRA6 reduces CNV production by inhibiting JAK2/STAT3 phosphorylation after circadian rhythm disturbance. The results suggest that STRA6 may be a new direction for the treatment of AMD.

Acknowledgments

Supported by the project of Research and Development of New Technologies and Systems for Low Vision Rehabilitation at Nantong University School of Medicine (23ZH313).

Authors Contributions: Y.Y. and S.Z. contributed equally to this work. Study concept and design: J.C. and A.S. Data collection and processing: Y.Y., S.Z., X.Y., and S.S. Technical and material support: Y.Y., S.Z., and S.S. Experiment implementation and date analysis: Y.Y., S.Z., and C.J. Paper writing: Y.Y. and S.Z. Funding support and study supervision: J.C. and A.S. All authors contributed to the study and approved the final manuscript.

Data Availability: The original contributions presented in the study are included in the article/Supplementary Material. The sequencing data have been deposited in the NCBI Gene Expression Omnibus (GEO) database under the accession code GSE253949. GEO records will be accessible with the following link after the indicated release date: https://www.ncbi.nlm.nih.gov/geo/query/acc.cgi?acc=GSE253949. The rest of the data included in the manuscript will be available from the corresponding author on reasonable request.

Disclosure: **Y. Yang**, None; **S. Zhang**, None; **S. Su**, None; **X. Yang**, None; **J. Chen**, None; **A. Sang**, None

References

1. Kawasaki R, Yasuda M, Song SJ, et al. The prevalence of age-related macular degeneration in Asians: a systematic review and meta-analysis. *Ophthalmology*. 2010;117(5):921–927.
2. Brown MM, Brown GC, Stein JD, et al. Age-related macular degeneration: economic burden and value-based medicine analysis. *Can J Ophthalmol*. 2005;40(3):277–287.
3. Nowak JZ. Age-related macular degeneration (AMD): pathogenesis and therapy. *Pharmacol Rep*. 2006;58(3):353–363.
4. Andreoli CM, Miller JW. Anti-vascular endothelial growth factor therapy for ocular neovascular disease. *Curr Opin Ophthalmol*. 2007;18(6):502–508.
5. Solomon SD, Lindsley K, Vedula SS, et al. Anti-vascular endothelial growth factor for neovascular age-related macular degeneration. *Cochrane Database Syst Rev*. 2014;8(8):CD005139.
6. Rao F, Xue T. Circadian-independent light regulation of mammalian metabolism. *Nat Metab*. 2024;6(6):1000–1007.
7. Dibner C, Schibler U, Albrecht U. The mammalian circadian timing system: organization and coordination of central and peripheral clocks. *Annu Rev Physiol*. 2010;72:517–549.
8. Chi-Castañeda D, Ortega A. Editorial: Disorders of circadian rhythms. *Front Endocrinol (Lausanne)*. 2020;11:637.
9. Patke A, Young MW, Axelrod S. Molecular mechanisms and physiological importance of circadian rhythms. *Nat Rev Mol Cell Biol*. 2020;21(2):67–84.
10. Curtis AM, Bellet MM, Sassone-Corsi P, et al. Circadian clock proteins and immunity. *Immunity*. 2014;40(2):178–186.
11. Mcmahon DG, Iuvone PM, Tosini G. Circadian organization of the mammalian retina: from gene regulation to physiology and diseases. *Prog Retin Eye Res*. 2014;39:58–76.
12. Liu X, Zhang Z, Ribelayga CP. Heterogeneous expression of the core circadian clock proteins among neuronal cell types in mouse retina. *PLoS One*. 2012;7(11):e50602.
13. Garita-Hernandez M, Lampič M, Chaffiol A, et al. Restoration of visual function by transplantation of optogenetically engineered photoreceptors. *Nat Commun*. 2019;10(1):4524.
14. Vallée A, Lecarpentier Y, Vallée R, et al. Circadian rhythms in exudative age-related macular degeneration: the key role of the canonical WNT/β-catenin pathway. *Int J Mol Sci*. 2020;21(3):820.
15. Young RW, Bok D. Participation of the retinal pigment epithelium in the rod outer segment renewal process. *J Cell Biol*. 1969;42(2):392–403.
16. Klettner A, Kampers M, Töbelmann D, et al. The influence of melatonin and light on VEGF secretion in primary RPE cells. *Biomolecules*. 2021;11(1):114.
17. Kawaguchi R, Yu J, Honda J, et al. A membrane receptor for retinol binding protein mediates cellular uptake of vitamin A. *Science*. 2007;315(5813):820–825.
18. Léveillard T, Sahel J-A. Metabolic and redox signaling in the retina. *Cell Mol Life Sci*. 2017;74(20):3649–3665.

19. Ruiz A, Mark M, Jacobs H, et al. Retinoid content, visual responses, and ocular morphology are compromised in the retinas of mice lacking the retinol-binding protein receptor, STRA6. *Invest Ophthalmol Vis Sci*. 2012;53(6):3027–3039.
20. Berry DC, Levi L, Noy N. Holo-retinol-binding protein and its receptor STRA6 drive oncogenic transformation. *Cancer Res*. 2014;74(21):6341–6351.
21. Kawaguchi R, Yu J, Wiita P, et al. An essential ligand-binding domain in the membrane receptor for retinol-binding protein revealed by large-scale mutagenesis and a human polymorphism. *J Biol Chem*. 2008;283(22):15160–15168.
22. Ransom J, Morgan PJ, Mccaffery PJ, et al. The rhythm of retinoids in the brain. *J Neurochem*. 2014;129(3):366–376.
23. Gliniak CM, Brown JM, Noy N. The retinol-binding protein receptor STRA6 regulates diurnal insulin responses. *J Biol Chem*. 2017;292(36):15080–15093.
24. Tan X, Takahashi H, Nishida J, et al. Excessive retinol intake exacerbates choroidal neovascularization through upregulated vascular endothelial growth factor in retinal pigment epithelium in mice. *Exp Eye Res*. 2015;131: 77–83.
25. Hicklin DJ, Ellis LM. Role of the vascular endothelial growth factor pathway in tumor growth and angiogenesis. *J Clin Oncol*. 2005;23(5):1011–1027.
26. Tsai H-C, Tzeng H-E, Huang C-Y, et al. WISP-1 positively regulates angiogenesis by controlling VEGF-A expression in human osteosarcoma. *Cell Death Dis*. 2017;8(4):e2750.
27. Apte RS, Chen DS, Ferrara N. VEGF in signaling and disease: beyond discovery and development. *Cell*. 2019;176(6):1248–1264.
28. Berry DC, O'byrne SM, Vreeland AC, et al. Cross talk between signaling and vitamin A transport by the retinol-binding protein receptor STRA6. *Mol Cell Biol*. 2012;32(15):3164–3175.
29. Zhang XS, Zhang P, Liu YH, et al. Caprylic acid improves lipid metabolism, suppresses the inflammatory response and activates the ABCA1/p-JAK2/p-STAT3 signaling pathway in C57BL/6J mice and RAW264.7 cells. *Biomed Environ Sci*. 2022;35(2):95–106.
30. Zeng H, Yang X, Liao K, et al. Circadian disruption reduces MUC4 expression via the clock molecule BMAL1 during dry eye development. *Exp Mol Med*. 2024;56(7):1655–1666.
31. Xie M, Tang Q, Nie J, et al. BMAL1-downregulation aggravates porphyromonas gingivalis-induced atherosclerosis by encouraging oxidative stress. *Circ Res*. 2020;126(6):e15–e29.
32. Tsuzuki K, Shimizu Y, Suzuki J, et al. Adverse effect of circadian rhythm disorder on reparative angiogenesis in hind limb ischemia. *J Am Heart Assoc*. 2021;10(16):e020896.
33. Ray S, Valekunja UK, Stangherlin A, et al. Circadian rhythms in the absence of the clock gene Bmal1. *Science*. 2020;367(6479):800–806.
34. Balsalobre A, Brown SA, Marcacci L, et al. Resetting of circadian time in peripheral tissues by glucocorticoid signaling. *Science*. 2000;289(5488):2344–2347.
35. Henning Y, Blind US, Larafa S, et al. Hypoxia aggravates ferroptosis in RPE cells by promoting the Fenton reaction. *Cell Death Dis*. 2022;13(7):662.
36. Balsalobre A, Damiola F, Schibler U. A serum shock induces circadian gene expression in mammalian tissue culture cells. *Cell*. 1998;93(6):929–937.
37. Gu M, Roy S, Raina K, et al. Inositol hexaphosphate suppresses growth and induces apoptosis in prostate carcinoma cells in culture and nude mouse xenograft: PI3K-Akt pathway as potential target. *Cancer Res*. 2009;69(24):9465–9472.
38. Pagani F, Trivedi A, Khatri D, et al. Silencing of pantothenate kinase 2 reduces endothelial cell angiogenesis. *Mol Med Rep*. 2018;18(5):4739–4746.
39. Bok D, Heller J. Transport of retinol from the blood to the retina: an autoradiographic study of the pigment epithelial cell surface receptor for plasma retinol-binding protein. *Exp Eye Res*. 1976;22(5):395–402.
40. Martínez-Águila A, Martín-Gil A, Carpena-Torres C, et al. Influence of circadian rhythm in the eye: significance of melatonin in glaucoma. *Biomolecules*. 2021;11(3):340.
41. Wiechmann AF, Summers JA. Circadian rhythms in the eye: the physiological significance of melatonin receptors in ocular tissues. *Prog Retin Eye Res*. 2008;27(2):137–160.
42. Bhatwadekar AD, Rameswara V. Circadian rhythms in diabetic retinopathy: an overview of pathogenesis and investigational drugs. *Expert Opin Investig Drugs*. 2020;29(12):1431–1442.
43. Ferris FL, Fine SL, Hyman L. Age-related macular degeneration and blindness due to neovascular maculopathy. *Arch Ophthalmol*. 1984;102(11):1640–1642.
44. Reppert SM, Weaver DR. Coordination of circadian timing in mammals. *Nature*. 2002;418(6901):935–941.
45. Bartness TJ, Goldman BD. Mammalian pineal melatonin: a clock for all seasons. *Experientia*. 1989;45(10):939–945.
46. Arendt J. Melatonin and the pineal gland: influence on mammalian seasonal and circadian physiology. *Rev Reprod*. 1998;3(1):13–22.
47. Xu Y, Cui K, Li J, et al. Melatonin attenuates choroidal neovascularization by regulating macrophage/microglia polarization via inhibition of RhoA/ROCK signaling pathway. *J Pineal Res*. 2020;69(1):e12660.
48. Jidigam VK, Sawant OB, Fuller RD, et al. Neuronal Bmal1 regulates retinal angiogenesis and neovascularization in mice. *Commun Biol*. 2022;5(1):792.
49. Jensen LD, Cao Y. Clock controls angiogenesis. *Cell Cycle*. 2013;12(3):405–408.
50. Bhutto I, Lutty G. Understanding age-related macular degeneration (AMD): relationships between the photoreceptor/retinal pigment epithelium/Bruch's membrane/choriocapillaris complex. *Mol Aspects Med*. 2012;33(4):295–317.
51. Martin ASKN, Leung M, Radhakrishnan R, et al. Vitamin A transporters in visual function: a mini review on membrane receptors for dietary vitamin A uptake, storage, and transport to the eye. *Nutrients*. 2021;13(11):3987.
52. Hagen E, Myhre AM, Smeland S, et al. Uptake of vitamin A in macrophages from physiologic transport proteins: role of retinol-binding protein and chylomicron remnants. *J Nutr Biochem*. 1999;10(6):345–352.
53. Agrón E, Mares J, Clemons TE, et al. Dietary nutrient intake and progression to late age-related macular degeneration in the age-related eye disease studies 1 and 2. *Ophthalmology*. 2021;128(3):425–442.

Investigative Ophthalmology & Visual Science